Scientific Research Publishing

Advances in Materials Physics and Chemistry, 2026, 16(11), 405-427
https://www.scirp.org/journal/ampc
ISSN Online: 2162-5328
ISSN Print: 2162-531X

Energy Band Gap and Refractive Index-Dependent Optical Properties of Nd^{3+}-Substituted Zinc Ferrite Nanoparticles

Shashi Kumar Jakkaraju[1,2], Katrapally Vijaya Kumar[1*]

[1]Department of Physics, JNTUH University College of Engineering Sultanpur, Sultanpur (V), Pulkal (M), Sangareddy (D), Telangana, India
[2]Department of Physics, Malla Reddy College of Engineering, Maisammaguda (V), Dulapally, Hyderabad, India
Email: *kvkphd@gmail.com

How to cite this paper: Jakkaraju, S.K. and Kumar, K.V. (2026) Energy Band Gap and Refractive Index-Dependent Optical Properties of Nd^{3+}-Substituted Zinc Ferrite Nanoparticles. *Advances in Materials Physics and Chemistry*, **16**, 405-427.
https://doi.org/10.4236/ampc.2026.1611023

Received: November 2, 2026
Accepted: November 24, 2026
Published: November 27, 2026

Copyright © 2026 by author(s) and Scientific Research Publishing Inc.
This work is licensed under the Creative Commons Attribution International License (CC BY 4.0).
http://creativecommons.org/licenses/by/4.0/

Open Access

Abstract

Nd^{3+} doped zinc ferrite nanoparticles with the chemical composition $ZnNd_xFe_{2-x}O_4$ (x = 0.00, 0.05, 0.10, 0.15, 0.20 and 0.25) were synthesized via the sol-gel auto-combustion method and their optical properties were studied to explore the effect of rare-earth inclusion on the electronic and dielectric response of the spinel lattice. From UV-Vis spectroscopic analysis, it is observed that the optical band gap decreased monotonously from 2.206 to 2.105 eV with the increase in doping concentration of Nd^{3+}, which may be associated with the influence of Nd^{3+}-related 4f electronic states near the conduction band, as suggested by previous literature. The refractive index (2.688 to 2.745), molar refractivity, molar electronic polarizability, dielectric polarizability, optical dielectric constant and optical susceptibility increased with increasing Nd^{3+} concentration. However, the velocity of light decreased, and the metallization criterion also decreased. The reflectivity and reflection loss increased, whereas the transmission decreased with an increase in refractive index. The optical basicity was found to increase with an increase in Nd^{3+} content, suggesting a more ionic nature of the cation-oxygen bond with similar oxygen packing density. The correlated results confirm that the electronic polarizability and optical response of $ZnFe_2O_4$ have been tuned up with Nd^{3+} doping due to local structural distortion and variation in the nature of the metal-oxygen bond.

Keywords

Zn-Nd Ferrite Nanoparticles, Optical Band Gap, Refractive Index, Derived Optical Properties

1. Introduction

Spinel ferrites have attracted considerable attention because their versatile structural, electrical, magnetic, dielectric, and optical properties make them promising materials for various technological applications. In particular, the optical response of ferrite nanoparticles is strongly associated with their electronic structure, chemical composition, density, and cationic environment. Optical characterisation therefore provides an important approach to understanding how electromagnetic radiation interacts with ferrite materials and to evaluating their suitability for optical and optoelectronic applications. Previous studies have demonstrated that the optical properties of ferrites can be systematically correlated with structural and compositional modifications of the material [1]-[4]. Among the different optical parameters, the optical band gap (E_g) and refractive index (μ) are particularly important for understanding the electronic and optical response of a material. The optical band gap represents the energy separation associated with electronic excitation and is sensitive to structural disorder, composition, density, and the local chemical environment. The refractive index, on the other hand, describes the propagation of electromagnetic radiation through the material and is closely related to its electronic polarizability. Barde *et al.* demonstrated that changes in optical band gap and refractive index can be used to establish correlations between composition, density, and other derived optical parameters in ferrite-based systems. [1] The refractive index has also been successfully estimated using different theoretical relationships, demonstrating its usefulness in predicting the optical response of ferrite materials [1] [5]-[11]. Reflectivity is another important optical parameter because it describes the fraction of incident electromagnetic radiation reflected at the material-air interface. Since reflectivity depends on refractive index, variations in μ are accompanied by corresponding changes in reflection loss and transmission coefficient. Previous investigations of ferrite-silica systems have shown that reflection loss, transmission coefficient, optical dielectric constant, dielectric polarizability, susceptibility, and metallization criterion exhibit mutually correlated variations because they depend directly or indirectly on the refractive index and optical band gap [1]. Thus, simultaneous evaluation of these parameters provides a more comprehensive understanding of the optical behavior than analysis of the refractive index or band gap alone. The molar refractive index (R_m) and molar electronic polarizability (α_m) provide further insight into the microscopic optical response of a material. The Lorentz-Lorenz relationship connects R_m with the refractive index and molar volume, while the molar electronic polarizability can subsequently be evaluated from R_m. The electronic polarizability represents the response of the electronic cloud to an applied electromagnetic field and is an important parameter for understanding the optical polarization of a material. Previous work has shown that electronic polarizability is closely associated with the optical band gap and refractive index, and that its variation can provide information about the electronic response and potential nonlinear optical behavior of ferrite-based materials [1] [12] [13]. The development of optical functional de-

vices including modulators, optical sensors, and memory devices also depends on electronic polarizability [1]. Optical basicity provides an additional means of evaluating the electronic character of oxide materials. It is related to the ability of oxide ions to donate electronic charge and is therefore associated with the polarizability and bonding character of the oxide network. Dimitrov and Komatsu established correlations between optical properties, electronic ion polarizability, and average single-bond strength in oxide materials, providing a useful framework for interpreting optical basicity and related parameters [3]. The optical basicity concept has also been applied to rare-earth-doped oxide systems to examine changes in electronic polarizability and the oxide-network environment.[4] Consequently, optical basicity can complement refractive-index and polarizability analyses when evaluating composition-induced modifications in oxide-based ferrites. The metallization criterion is another useful parameter for assessing changes in the electronic character of a material. Because the metallization criterion is related to the optical band gap, refractive index, and density, its variation can be correlated with changes in the electronic structure of the material. In the ferrite-silica system reported by Barde *et al.*, the simultaneous variation of the metallization criterion with refractive index and optical band gap demonstrated the strong interdependence of the optical parameters [1]. Such relationships are particularly useful for evaluating whether compositional modification produces changes toward more insulating or more optically polarizable electronic behavior. Optical packing density (OPD) provides complementary structural information because it is associated with the packing of oxygen within the oxide network. In the previously reported lithium ferrite-silica system, changes in OPD were correlated with changes in density, lattice parameters, and silica incorporation. [1] Therefore, OPD, together with optical basicity, metallization criterion, molar refractive index, and electronic polarizability, can provide a broader picture of the relationship between structural modification and optical response. Rare-earth substitution provides an effective route for modifying the optical characteristics of ferrites because rare-earth ions differ from Fe^{3+} in ionic size, electronic configuration, and bonding characteristics. In the present system, Nd^{3+} substitution is expected to modify the local structural and electronic environment of $ZnFe_2O_4$. The larger Nd^{3+} ion can introduce changes in the lattice and cationic environment, which may consequently influence the optical band gap, refractive index, reflectivity, polarizability, and other derived optical parameters. Therefore, systematically investigating these mutually related quantities is useful for establishing composition-structure-optical-property relationships in Nd-substituted zinc ferrite nanoparticles.

The present work focuses on the systematic investigation of the optical properties of $ZnNd_xFe_{2-x}O_4$ ferrite nanoparticles with x = 0.00, 0.05, 0.10, 0.15, 0.20, and 0.25. Particular attention is given to the optical band gap (E_g), refractive index (μ), reflectivity (R), molar refractive index (R_m), molar electronic polarizability (α_m), optical basicity, metallization criterion, and optical packing density (OPD). The

interrelationships among these parameters are examined to understand how Nd^{3+} incorporation modifies the optical response of the $ZnFe_2O_4$ lattice. The approach follows the optical-parameter framework established for ferrite-based systems, in which the experimentally accessible band gap and density are used to derive and correlate a series of related optical quantities [1] [3] [4] [14] [15]. This systematic analysis provides a comprehensive understanding of the composition-dependent optical behavior of Nd-doped zinc ferrite nanoparticles and its relevance to optical, nonlinear-optical, photonic, and optoelectronic applications.

2. Experimental

2.1. Materials and Synthesis

Nd^{3+}-doped zinc ferrite nanoparticles with the general formula $ZnNd_xFe_{2-x}O_4$ (x = 0.00, 0.05, 0.10, 0.15, 0.20, and 0.25) were synthesized via the sol-gel auto-combustion method. Zinc nitrate hexahydrate [$Zn(NO_3)_2{\cdot}6H_2O$, 99%], ferric nitrate nonahydrate [$Fe(NO_3)_3{\cdot}9H_2O$, 98%], and neodymium nitrate hexahydrate [$Nd(NO_3)_3{\cdot}6H_2O$, 99%] were used as metal precursors, while citric acid monohydrate [$C_6H_8O_7{\cdot}H_2O$, AR grade, Sigma-Aldrich] served as the chelating agent and fuel, with a total metal-ion-to-citric acid molar ratio of 1:3. Stoichiometric amounts of the precursors were dissolved separately in a minimum volume of double-distilled water and then combined under continuous magnetic stirring to obtain a homogeneous precursor solution. The pH of the mixture was adjusted to ~7 by the dropwise addition of aqueous ammonia. The resulting solution was heated at 80˚C on a magnetic hot plate with constant stirring until excess water evaporated, yielding a viscous brown gel. On further heating to ~200˚C, the gel underwent spontaneous self-ignition, resulting in a rapid auto-combustion reaction that produced a voluminous, porous precursor powder. This powder was ground into a fine, homogeneous form using an agate mortar and pestle and subsequently calcined in air at 700˚C for 4 h to remove residual organic matter, enhance crystallinity, and promote the formation of a single-phase spinel ferrite structure. The calcined samples were cooled naturally to room temperature prior to characterization.

2.2. Characterizations

The optical absorption spectra of the $ZnNd_xFe_{2-x}O_4$ ferrite nanoparticles were recorded over 190 - 1100 nm using a Cary 60 UV-Visible spectrophotometer in double-beam mode at a data acquisition rate of 80 points per second. Approximately 100mg of barium sulphate ($BaSO_4$) was initially placed in the sample holder, and the synthesized powder sample of 20 mg was carefully spread over the $BaSO_4$ layer to obtain a uniform surface. Pure $BaSO_4$ was used as the reference material in the reference beam. The diffuse reflectance spectra were recorded over the desired wavelength range to investigate the optical properties of the synthesized nanoferrite samples. The measured reflectance data were subsequently used to evaluate the optical band gap energy and related optical parameters.

3. Results and Discussion

3.1. Structural Properties

The structural properties of the $ZnNd_xFe_{2-x}O_4$ (x = 0.00, 0.05, 0.10, 0.15, 0.20 and 0.25) ferrite nanoparticles, including FTIR, thermal analysis, magnetic and cation distribution, have been reported by Kumar *et al.* [16]. A representative subset is presented here to establish the phase and the structural parameters used in the optical analysis. Figure 1 shows the XRD patterns of the undoped (x = 0.00) and doped (x = 0.05, 0.10, 0.15, 0.20, and 0.25) samples [16]. As listed in Table 1, the lattice parameter increases overall from 8.4447 to 8.4495 Å (V = 602.22 to 603.24 $Å^3$), consistent with the partial replacement of Fe^{3+} (0.645 Å) by the larger Nd^{3+} (0.983 Å). However, the trend is not strictly monotonic. The crystallite size decreases from 40.95 to 33.01 nm, while the microstrain increases from 3.15×10^{-3} to 4.29×10^{-3}, indicating growing lattice distortion. The X-ray density increases from 5.318 to 5.867 $g \cdot cm^{-3}$, mainly because the heavier Nd replaces Fe at nearly

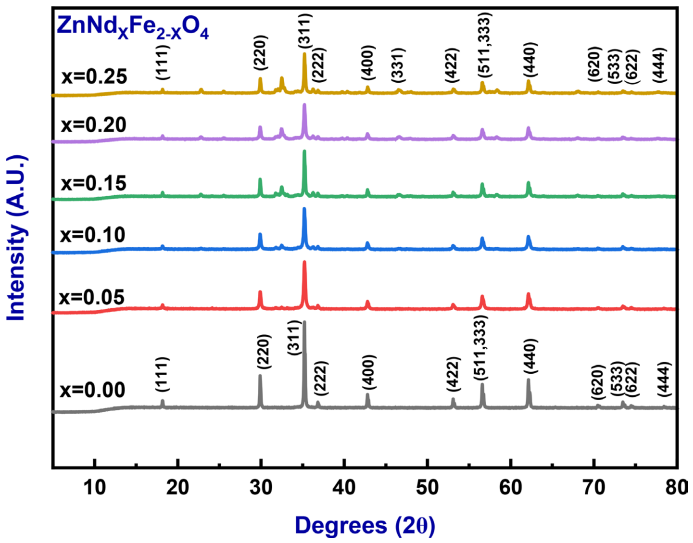


Figure 1. XRD patterns of $ZnNd_xFe_{2-x}O_4$ (x = 0.00, 0.05, 0.10, 0.15, 0.20, and 0.25) ferrite nanoparticles, Kumar *et al.* [16].

Table 1. Structural parameters of $ZnNd_xFe_{2-x}O_4$ (x = 0.00,0.05,0.10,0.15,0.20 and 0.25) ferrite nanoparticles, Kumar *et al.* [16].

Concentration (x)	Crystallite size D (nm)	lattice parameter a (Å)	Volume V ($Å^3$)	Lattice strain ε (10^{-3})	Dislocation Density δ (10^{-4} nm^{-2})	X-Ray density D_x (gm/cm^3)	d-spacing d (Å)
0.00	40.95	8.4447	602.22	3.1493	5.9634	5.318	2.5462
0.05	39.34	8.4482	602.97	3.2708	6.4615	5.423	2.5472
0.10	35.64	8.4497	603.29	3.7417	7.8727	5.532	2.5477
0.15	38.78	8.4485	603.03	3.4719	6.6494	5.646	2.5473
0.20	34.41	8.4494	603.22	3.8515	8.4456	5.756	2.5476
0.25	33.01	8.4495	603.24	4.2900	9.1772	5.867	2.5476

constant cell volume, and it enters the molar volume ($V_m = Mw/\rho_x$) and the Anderson-Schreiber relation used below. As the crystallite sizes (33 - 41 nm) are well above the quantum-confinement regime, the optical band-gap changes are more plausibly linked to Nd-related 4f states, lattice distortion, and defect states than to size effects.

3.2. Optical Band Gap (E_g) (UV-Vis)

The optical behavior and changes in energy band gap (E_g) of Nd^{3+}-doped zinc ferrite nanoparticles were studied by measuring ultraviolet-visible (UV-Vis) absorbance across the 200 - 1000 nm wavelength range using a UV-Vis spectrophotometer. The absorption spectra of $ZnNd_xFe_{2-x}O_4$ (x = 0.00, 0.05, 0.10, 0.15, 0.20 and 0.25) ferrite nanoparticles are illustrated in **Figures 2(a)-(f)**. It is evident that the intensity of absorption is greater at shorter wavelengths but gradually decreases as the wavelength increases. Eventually, the absorption approaches saturation, resulting in minimal absorption. In ferrites, the absorbance in the visible region results from the excitation of transition electrons from the O-2p (valence band) to the Fe-3d (conduction band) level. The optical band gap energy of the Nd doped zinc ferrite nanoparticles was determined using the Tauc relation, assuming a direct allowed electronic transition. Tauc plots were constructed by plotting $(\alpha h\nu)^2$ against photon energy ($h\nu$), and the optical band gap energy (E_g) was obtained by extrapolating the linear portion of each plot to the photon-energy axis. The corresponding relationship is expressed by Equation (1) [17].

$$(\alpha h\nu)^2 = A(h\nu - E_g) \tag{1}$$

where E_g denotes the optical energy band gap value, α is the absorption coefficient, A is a constant, h is the Planck constant, and ν is the light frequency. The optical band gap values were determined using the Tauc method by considering the linear region of the corresponding plots. The same analysis approach was consistently applied to all samples to ensure a reliable comparison of the composition-dependent optical properties. The optical band gap values were estimated by drawing tangents at the x-axis of the Tauc plot. **Table 2** contains the values of the UV-Vis parameters. The energy band gap values decreased progressively from 2.206 to 2.105 eV with increasing Nd^{3+} doping concentration in zinc ferrite nanoparticles. The maximum band gap was observed in the undoped zinc ferrite nanoparticles, attributed to effective orbital overlap between Fe-3d and O2-p energy states. Upon Nd^{3+} ion incorporation, the band gap narrows due to the introduction of Nd^{3+} 4f energy states just below the conduction band [18]. These 4f states interact with the O2-p valence band orbitals, enhancing charge migration from the Nd^{3+} energy states to the zinc ferrite conduction band. However, the present UV-Vis measurements provide information about the optical absorption characteristics and estimated band gap energies of the samples but do not directly establish the energy positions of Nd 4f states or their orbital interactions with the Fe 3d and O 2p states. Therefore, the possible contribution of Nd 4f-related states to

the observed optical transitions is considered a literature-supported interpretation [19] [20]. The band gap has several physical properties, one of which is the steepness parameter (σ_{st}), which describes the broadening of the absorption edge

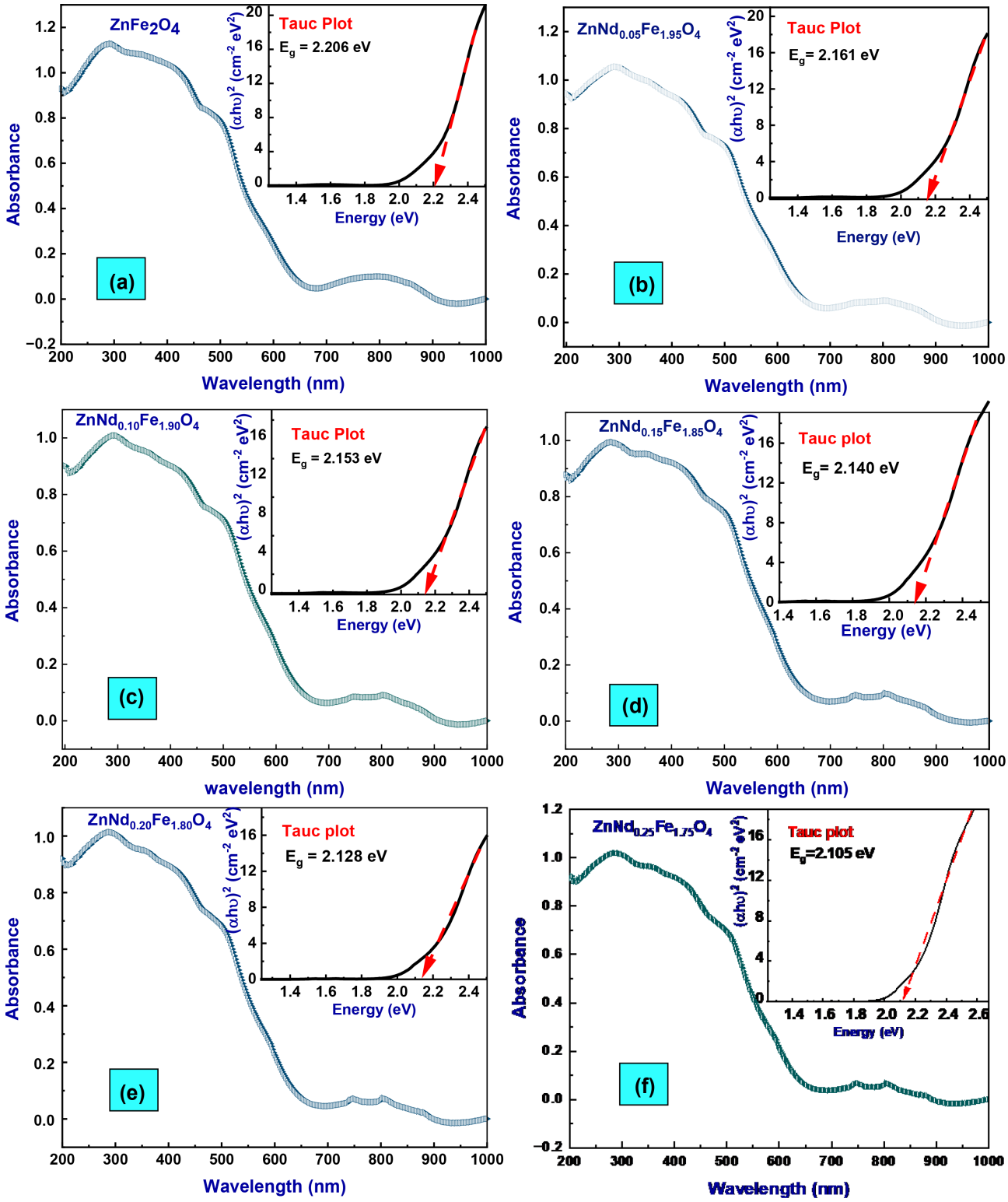


Figure 2. Energy band gap Graphs of Nd doped $ZnNd_xFe_{2-x}O_4$ (x = 0.00, 0.05, 0.10, 0.15, 0.20, 0.25) ferrite nanoparticles.

Table 2. Energy band gap, propagation speed of light in material, reflectivity, absorption coefficient, molar refractive index and electronic polarizability of $ZnNd_xFe_{2-x}O_4$ ferrite nanoparticles.

x	E_g (eV)	V × 10^{10} (cm/s)	R (%)	α (cm^{-1})	R_m (cm^3/mol)	α_m (Å^3)	α_D (Å^3)
0.00	2.206	1.1153	20.950	1.4913	30.590	12.127	11.417
0.05	2.161	1.1062	21.246	1.4596	30.816	12.217	11.524
0.10	2.153	1.1038	21.326	1.4512	30.882	12.243	11.555
0.15	2.140	1.1004	21.437	1.4396	30.939	12.265	11.585
0.20	2.128	1.0973	21.540	1.4290	31.012	12.294	11.620
0.25	2.105	1.0922	21.709	1.4118	31.121	12.337	11.673

due to electron-phonon interactions [21]. It is calculated by the following formula [22]

$$\sigma_{st} = \frac{k_B T}{E_g} \tag{2}$$

where T is the room temperature, and k_B is the Boltzmann constant. Furthermore, the strength of the electron-photon interaction, E_{e-ph}, can be obtained from the following relation, which is inversely proportional to the steepness parameter [23].

$$E_{e-ph} = \frac{2}{3\sigma_{st}} \tag{3}$$

The ferrite nanoparticles showed a slight increase in steepness and a decrease in electron-phonon interaction potential, which reveals that the doping seems to enhance the crystalline quality and diminish the density of some of the structural defects in the prepared ferrite nanoparticles [24]. Rekaby *et al.* noticed similar findings when tailoring the structural, optical and magnetic properties of $Co_{0.6}Zn_{0.4}Fe_2O_4$ by co-doping Ni^{2+}-Al^{3+}, which had enhanced crystalline quality due to the increase in the steepness parameter and the decrease in the electron-phonon interaction potential [25].

3.3. Refractive Index (μ)

With the help of the energy gap, one can find the refractive index of the sample. The refractive index (μ) is an important optical parameter that provides information about the interaction of electromagnetic radiation with a material and its associated electronic polarizability. Along with the optical energy band gap E_g, the refractive index plays a significant role in understanding and predicting the optical response of materials and is therefore relevant to the development of linear and nonlinear optical devices, including integrated optical components, optical switches, filters, and modulators [26]. Experimentally, the refractive index can be determined using techniques such as ellipsometry. However, in the absence of direct measurements, μ can be estimated from empirical and semi-empirical relationships involving the optical band gap and other material parameters [26]-[29].

In the present study, we estimated the refractive index using several established models to obtain a reliable representation of the optical response. The relations employed include the Anderson-Schreiber, Dimitrov-Sakka, Moss, Herve-Vandamme, Ravindra *et al.*, Reddy-Ahammed, Dionne-Woolley, Reddy-Anjaneyulu, and Anani *et al.* models, expressed as follows:

$$\text{Anderson-Schreiber:}\quad \mu = 1 + 0.207\rho_x \tag{4}$$

$$\text{Dimitrov-Sakka:}\quad 1 - \sqrt{\frac{E_g}{20}} = \frac{\mu^2 - 1}{\mu^2 + 2} \tag{5}$$

$$\text{Moss:}\quad \mu^4 \times E_g = 95\text{eV} \tag{6}$$

$$\text{Herve-Vandamme:}\quad \mu^2 = 1 + \left(\frac{A}{E_g + B}\right)^2 \tag{7}$$

$$\text{Ravindra } et\ al.:\quad \mu = 4.16 - 1.12E_g + 0.31E_g^2 - 0.08E_g^3 \tag{8}$$

$$\text{Reddy-Ahammed:}\quad \mu^4(E_g - 0.365) = 154 \tag{9}$$

$$\text{Dionne-Woolley:}\quad \mu^2 = -11.63\ln E_g + 19.19 \tag{10}$$

$$\text{Reddy-Anjaneyulu:}\quad E_g e^{\mu} = 36.3 \tag{11}$$

$$\text{Anani } et\ al:\quad \mu = \frac{17 - E_g}{5} \tag{12}$$

where E_g is expressed in eV, ρ_x represents X-ray density, the corresponding material parameters in the Anderson-Schreiber relation, and A and B are constants associated with the Herve-Vandamme model. Here, A corresponds approximately to the ionization energy of hydrogen (13.6 eV), whereas B is an empirical constant of approximately 3.47 eV, representing the energy difference between the ultraviolet resonance energy and the optical band gap energy. The use of multiple empirical models provides a comparative estimation based on different relationships between refractive index and the optical, electronic, and dielectric characteristics of materials, thereby avoiding exclusive reliance on a single empirical relationship. These models were considered as approximate estimation approaches for the investigated Nd doped zinc ferrite nanoparticles system, which is a spinel oxide semiconductor. The average of the nine predicted values was adopted as a representative refractive-index estimate for subsequent calculations. The calculated refractive-index values obtained from the different theoretical models, together with their corresponding average values, are presented in **Table 3** and in **Figures 3(a)-(j)**. The use of multiple empirical relations provides a comparative assessment of the refractive response and minimizes dependence on any single approximation. The refractive index increases from 2.6881 for x = 0.00 to 2.7448 for x = 0.25. The variation in the refractive index μ with Nd^{3+} content follows the corresponding variation in the optical band gap E_g demonstrating the strong interdependence between the electronic structure and optical response of the investigated materials. The calculated refractive-index values for all compositions

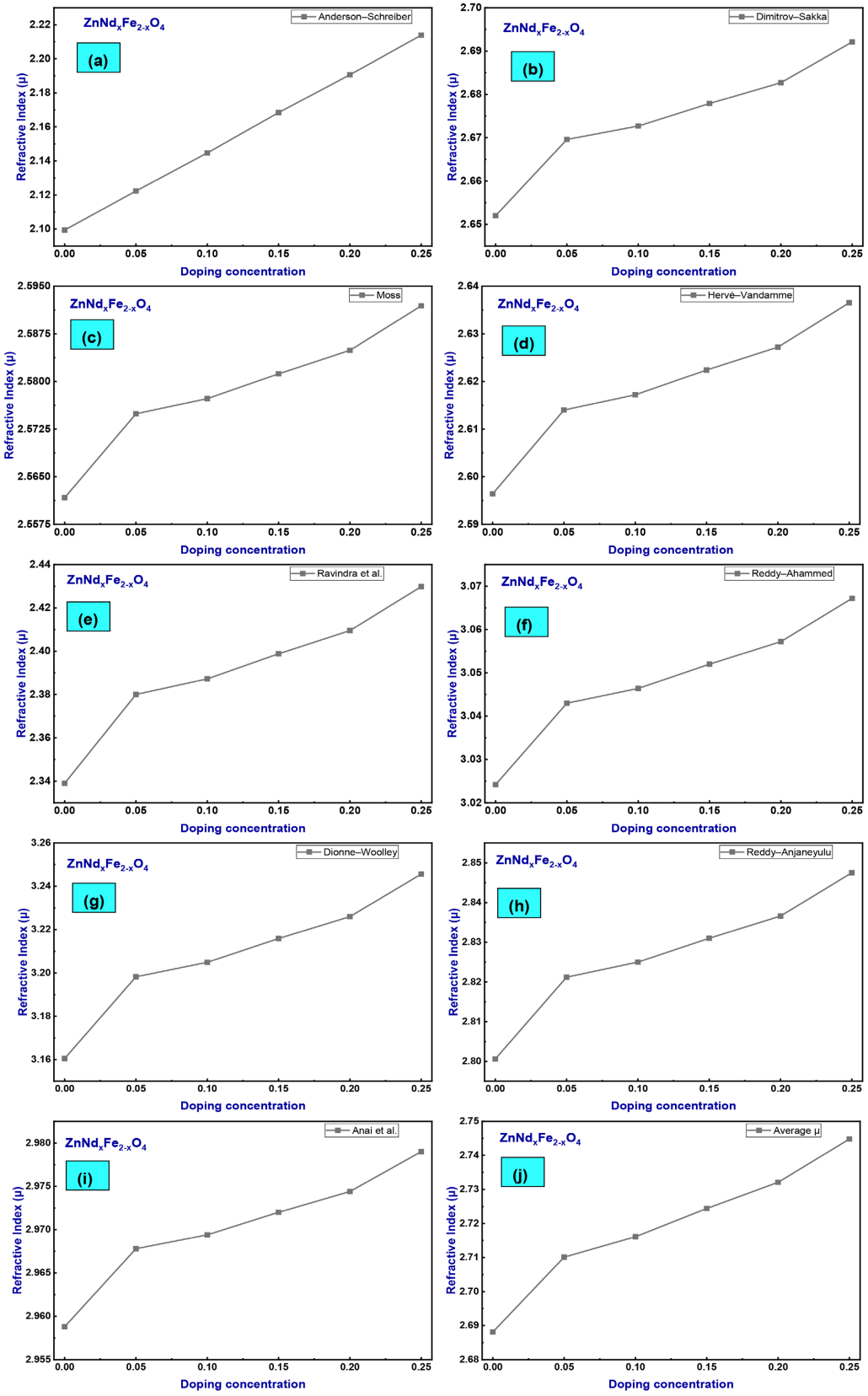


Figure 3. Refractive index graphs of Nd doped $ZnNd_xFe_{2-x}O_4$ (x = 0.00, 0.05, 0.10, 0.15, 0.20, 0.25) ferrite nanoparticles using various models.

Table 3. Refractive indices of $ZnNd_xFe_{2-x}O_4$ ferrite nanoparticles obtained from different theoretical models.

x	Anderson-Schreiber	Dimitrov-Sakka	Moss	Hervé-Vandamme	Ravindra *et al.*	Reddy-Ahammed	Dionne-Woolley	Reddy-Anjaneyulu	Anai *et al.*	Average μ
0.00	2.0994	2.6520	2.5617	2.5964	2.3390	3.0242	3.1605	2.8006	2.9588	2.6881
0.05	2.1223	2.6696	2.5749	2.6140	2.3800	3.0430	3.1982	2.8212	2.9678	2.7101
0.10	2.1447	2.6727	2.5773	2.6172	2.3872	3.0464	3.2049	2.8250	2.9694	2.7161
0.15	2.1684	2.6779	2.5812	2.6224	2.3988	3.0520	3.2159	2.8310	2.9720	2.7244
0.20	2.1906	2.6827	2.5849	2.6272	2.4095	3.0572	3.2260	2.8366	2.9744	2.7321
0.25	2.2139	2.6921	2.5919	2.6365	2.4298	3.0672	3.2456	2.8475	2.9790	2.7448

exhibit a monotonic increase with increasing Nd^{3+} concentration. In general, a lower optical band gap is associated with a higher refractive index, indicating enhanced interaction between the incident electromagnetic field and the polarizable constituents of the ferrite. This behavior is consistent with the reduction in E_g, as a smaller separation between the relevant electronic states generally facilitates stronger electronic polarization at optical frequencies. The observed increase in μ can therefore be associated with enhanced electronic polarizability and a reduced effective photon energy required for electronic transitions. Furthermore, the accompanying increase in molar refractivity and electronic polarizability supports this interpretation. The refractive index depends on the electronic polarizability of the constituent ions and the structural environment of the material, including the lattice parameter and the valence-electron contribution of the constituent atoms. Incorporation of the relatively large Nd^{3+} ions into the $ZnFe_2O_4$ lattice can induce lattice expansion and modify the local cation-oxygen environment and charge distribution. These structural changes can influence the displacement of bound electrons under an applied optical field, thereby enhancing the refractive response. Thus, the increase in μ is not merely a numerical consequence of the empirical relations used for its estimation but reflects the progressive modification of the electronic polarizability and optical density of the ferrite matrix. A similar increase in refractive index associated with Nd-induced polarizability and lattice expansion has been reported for Nd-doped $GdVO_4$ by Soharab *et al.* [30]. The Nd-doped zinc ferrite nanoparticles with a narrow band gap may be suitable for photocatalytic applications under visible light [31] and hydrogen generation from solar water splitting [32].

3.4. Velocity of Light (v)

The velocity of electromagnetic radiation inside the ferrite decreases from 1.1153×10^{10} to 1.0922×10^{10} cm·s^{-1} as x increases from 0.00 to 0.25, as depicted in Table 2. The velocity is calculated from $v = c/\mu$, where c is the velocity of light in a vacuum. Consequently, the decrease is the direct reciprocal response to the increase in refractive index. The physical significance of this parameter is that electromagnetic waves propagate more slowly in a medium with a higher refractive index

because the oscillating electric field interacts more strongly with the bound charges of the material. The gradual decrease in v therefore indicates enhanced electromagnetic retardation associated with the Nd-substituted ferrite matrix. This behavior is consistent with the increasing polarizability and optical dielectric response. Although the calculated change is relatively small, its systematic nature demonstrates that Nd substitution measurably modifies the optical propagation characteristics.

3.5. Reflectivity (R)

The reflectivity is calculated using [33]

$$R = \left(\frac{\mu_{material} - \mu_{air}}{\mu_{material} + \mu_{air}} \right)^2 \times 100\% \Rightarrow R = \left(\frac{\mu_{material} - 1}{\mu_{material} + 1} \right)^2 \times 100\% \quad (13)$$

Reflectivity describes the fraction of incident optical radiation returned from the material surface due to the difference between the optical properties of the ferrite and the surrounding medium. It can be observed that R increases progressively from 20.95% for the undoped $ZnFe_2O_4$ sample to 21.709% for x = 0.25. Table 2 shows that the variation is consistent with the corresponding monotonic increase in the refractive index with Nd^{3+} concentration. Since reflectivity at the sample-air interface is directly dependent on the refractive index, an increase in μ results in a larger optical impedance mismatch between the ferrite and the surrounding medium, thereby increasing the fraction of incident electromagnetic radiation reflected from the surface. The increase in refractive index can be associated with the enhanced electronic polarizability and modification of the local cation-oxygen environment induced by Nd^{3+} incorporation. The relatively larger Nd^{3+} ion can also promote lattice expansion and modify the charge distribution within the ferrite lattice, influencing the response of bound electrons to the incident optical field. Consequently, the progressive increase in optical polarizability and refractive index leads to a corresponding increase in reflectivity. Thus, the observed reflectivity variation indicates that Nd substitution influences not only the propagation of electromagnetic radiation within the ferrite matrix but also its interaction with the sample surface. The relatively small change in R from 20.950% to 21.709% suggests a gradual modification of the surface optical response rather than an abrupt change. Such optical behavior may be relevant to the consideration of Nd-doped $ZnFe_2O_4$ ferrite nanoparticles in optical coatings, electromagnetic-interaction layers, and frequency-dependent optical components, although further application-specific investigations would be required.

3.6. Absorption Coefficient (α)

The Kubelka-Munk function, F(R), was calculated from the reflectivity R of $ZnNd_xFe_{2-x}O_4$ ferrite nanoparticles using the following approach reported by N. P. Barde *et al.* [34] [35]

$$\alpha = F(R) = \frac{(1-R)^2}{2R} \tag{14}$$

where R is the fractional reflectivity of the material. The reflectivity $R = \left(\frac{\mu-1}{\mu+1}\right)^2$ values were estimated from the refractive index using the relation discussed in the preceding section. The calculated absorption coefficient values are presented in Table 2. As the Nd^{3+} concentration increases from x = 0.00 to 0.25, α decreases from 1.4913 to 1.4118. This gradual decrease indicates a change in the optical absorption response of the ferrite nanoparticles with Nd^{3+} substitution. Such variation may be associated with modifications in the refractive index and the local structural environment arising from the substitution of Fe^{3+} ions by larger Nd^{3+} ions. The resulting lattice distortion and structural strain may influence the optical response of the material [16].

3.7. Molar Refractivity (R_m) and Molar Electronic Polarizability (α_m)

Variation of Molar refractivity (R_m) and molar electronic polarizability (α_m) is calculated using equations [12] [13]

$$R_m = \frac{\mu^2 - 1}{\mu^2 + 2}\frac{M_w}{\rho_x} \tag{15}$$

where molar volume $V_m = M_w/\rho_x$

$$\alpha_m = \frac{3R_m}{4\pi N} \tag{16}$$

Polarizability describes how a material's electron cloud responds to an applied electromagnetic field. The calculated molar electronic polarizability (α) exhibits a direct relationship with the molar refractivity (R_m). As presented in Table 2, (α) increases from 12.127 to 12.337 $Å^3$ with an increase in Nd^{3+} concentration from (x = 0.00) to (x = 0.25). This enhancement is associated with changes in the optical band gap energy. Generally, electronic polarizability increases as the optical band gap decreases, since less energy is required to induce electronic transitions. In the present study, the band gap decreases from 2.206 eV to 2.105 eV with increasing Nd^{3+} content. This reduction may facilitate a stronger electronic response to incident electromagnetic radiation and increase the deformability of the electron cloud within the metal-oxygen network. Such changes in electronic polarizability can significantly influence the nonlinear optical response of the material. When light interacts with the material, the induced electronic polarization contributes to its nonlinear optical behaviour. These properties are also associated with parameters such as the refractive index, metal-ion concentration, and electro-optic response. Understanding these relationships is important for evaluating the potential of the investigated materials in optical applications, including optical modulators, sensors, and memory devices.

3.8. Dielectric Polarizability (α_D)

The dielectric polarizability increases from 11.417 to 11.673 Å^3 over the investigated composition range depicted in Table 2. Dielectric polarizability represents the ability of the charge distribution within the material to be displaced in response to an applied electric field. [36]

$$\alpha_D = \frac{1}{\mathrm{b}} \mathrm{V}_m \frac{\varepsilon' - 1}{\varepsilon' + 2} \tag{17}$$

At optical frequencies, the dominant contribution is associated primarily with electronic polarization. The increase in α_D indicates that Nd substitution progressively modifies the local charge distribution and the metal-oxygen bonding environment. The larger ionic size of Nd^{3+} can perturb the surrounding oxygen coordination and alter the local electric field experienced by neighboring ions. The progressive increase in dielectric polarizability may partly be associated with the enhanced lattice strain induced by the substitution of the relatively large Nd^{3+} ions at Fe^{3+} sites. The reduction in crystallite size with Nd^{3+} incorporation increases the relative contribution of surface and defect-associated regions, which may additionally influence the dielectric polarization. Such changes can influence the displacement of electronic charge under an optical field and consequently increase the polarizability. The trend in α_D is consistent with the increases in refractive index, optical dielectric constant and optical susceptibility. These parameters therefore provide complementary descriptions of the same underlying enhancement in the optical polarization response.

3.9. Reflection Loss (R_L) and Transmission (T)

The reflection loss parameter increases from 0.2095 to 0.2171, whereas the transmission decreases from 0.6536 to 0.6433 with increasing Nd content.[36]

$$R_{\mathrm{L}} = \left(\frac{\mu - 1}{\mu + 1} \right)^2 \tag{18}$$

$$T = \frac{2\mu}{\mu^2 + 1} \tag{19}$$

These parameters describe complementary aspects of the interaction between incident radiation and the ferrite material. Reflection loss is associated with radiation reflected from the material surface, while transmission represents the fraction of incident radiation that passes through the material. The increase in R_L is consistent with the higher refractive index and the resulting increase in optical mismatch at the interface. In parallel, the decrease in T indicates that a smaller fraction of incident radiation is transmitted through the sample. In contrast, the calculated transmission (T) exhibits a slight decrease with increasing Nd^{3+} concentration. This variation represents the response predicted by the adopted simplified optical model, since the model does not explicitly account for the absorption coefficient or sample thickness. Thus, the observed changes in R_L and T indicate variations in the estimated interfacial and transmission-related optical re-

sponses of the ferrite system with Nd^{3+} substitution. These trends may be associated with modifications in the optical parameters arising from changes in the electronic and structural characteristics of the material. The calculated values of reflection loss (R_L) and transmission (T) are presented in Table 4.

Table 4. Variation of reflection and transmission loss, optical dielectric constant, electric susceptibility, Metallization criterion, Ionic concentration of Nd, oxygen packing density, and optical basicity of $ZnNd_xFe_{2-x}O_4$ ferrite nanoparticles.

x	R_L	T	p	χ	M(μ)	M (E_g)	N × 10^{21} (cm^{-3})	OPD	Λth
0.00	0.2095	0.6536	6.2259	0.4954	0.3252	0.3321	0	88.241	0.780
0.05	0.2125	0.6495	6.3446	0.5049	0.3210	0.3287	0.6634	88.130	0.787
0.10	0.2133	0.6485	6.3772	0.5075	0.3199	0.3281	1.3261	88.087	0.794
0.15	0.2144	0.6469	6.4224	0.5111	0.3184	0.3271	1.9900	88.123	0.800
0.20	0.2154	0.6456	6.4644	0.5144	0.3170	0.3262	2.6526	88.097	0.807
0.25	0.2171	0.6433	6.5339	0.5200	0.3147	0.3244	3.3154	88.087	0.814

3.10. Optical Dielectric Constant (p)

The optical dielectric constant, calculated from [15]

$$p = \mu^2 - 1 \tag{20}$$

The value increases from 6.2259 to 6.5339 with increasing Nd^{3+} content, as shown in Table 4. The optical dielectric constant characterizes the ability of the material to respond to the electric component of electromagnetic radiation and provides a measure of its optical-frequency polarization response. Because p depends directly on the square of the refractive index, its increase reflects the corresponding rise in μ obtained from the optical measurements. Physically, this enhancement suggests a stronger induced polarization under the optical field. The decrease in E_g and the increase in electronic polarizability provide a consistent microscopic basis for this behavior. The larger optical dielectric response indicates that the electronic charge distribution within the Nd-substituted ferrite becomes increasingly responsive to high-frequency electromagnetic excitation. The systematic variation of p thus demonstrates that Nd^{3+} concentration can be used as a compositional parameter for tuning the optical dielectric response of $ZnNd_xFe_{2-x}O_4$ ferrite nanoparticles.

3.11. Optical Susceptibility (χ)

The electrical susceptibility can also be estimated from the refractive index using the following relationship. [37]

$$\chi = \frac{\mu^2 - 1}{4\pi} \tag{21}$$

Susceptibility quantifies a material's ability to undergo polarization in response to an applied external field, and whereas its value in vacuum is $\chi = 0$, it provides a more direct measure of the electromagnetic wave-matter interaction than a re-

fractive index alone. The obtained measurements show that χ increases from 0.4954 to 0.5200 as the Nd^{3+} content increases from x = 0.00 to x = 0.25, indicating that the electronic charge distribution becomes progressively more responsive to the optical electric field. This behavior is consistent with the simultaneous increase in refractive index, optical dielectric constant, and electronic polarizability. At microscopic scale, mobile charge carriers within the sample perturb the incident electromagnetic wave in proportion to the material's electric susceptibility; the resulting electron-electromagnetic wave interaction generates secondary waves whose phase relationships govern properties such as dispersion, absorption, and polarization. Physically, Nd^{3+} substitution modifies the local metal-oxygen bonding and charge environment, allowing progressively greater induced polarization under optical excitation. The increase in χ correspondingly implies that the velocity of electromagnetic waves through the material is hindered to a greater extent, consistent with the decrease in V from 1.1153×10^{10} to 1.0922×10^{10} cm/s (Table 2). The gradual, monotonic variation of χ across the series further indicates that Nd^{3+} substitution produces a controlled, systematic modification of the optical polarization response rather than a discontinuous electronic transformation.

3.12. Ionic Concentration (N)

The concentration of Nd^{3+} ions in the sample can be estimated using the following relationship. [15]

$$N = \frac{X_{Nd}\rho N_A}{M_w} \tag{22}$$

where X_{Nd} represents the molar fraction, and ρ is the density of Nd^{3+}, while N_A denote Avogadro's number and Mw is the molecular weight of the sample. The estimated ionic concentration is presented in Table 4 and are consistent with the proposed stoichiometry for the system, *i.e.*, the obtained values of N increase from 0 to 3.3154×10^{21} cm^{-3} with increasing Nd^{3+} content from x = 0.00 to x = 0.25. This systematic increase confirms the progressive and controlled incorporation of Nd^{3+} into the $ZnFe_2O_4$ lattice, in agreement with the intended compositional design of the series. Consequently, the variation in N provides a useful compositional basis for correlating the concentration of substituted ions with changes in *Eg*, refractive index, polarizability and other optical parameters.

3.13. Metallization Criterion

Metallization criterion (M) is used to assess the electronic nature of a material and its tendency towards metallic or insulating behaviour. Materials with $R_m/V_m \geq 1$ are generally associated with metallic characteristics, whereas values below unity indicate predominantly non-metallic behavior, *i.e.*, good insulators. Based on this criterion, all compositions investigated in the present study exhibit insulating characteristics, consistent with the typical electrical behavior of ferrite materials. The metallization criterion can be estimated from the refractive index of the material (μ) and the energy gap (E_g) using the following equation [15].

$$M(\mu) = 1 - \frac{R_m}{V_m} \tag{23}$$

$$M(E_g) = \sqrt{\frac{E_g}{20}} \tag{24}$$

Metallization criterion values calculated using both approaches are presented in Table 4. The data reveal a decreasing trend in M irrespective of the calculation method with increasing Nd^{3+} content, from 0.3252 to 0.3147 for M(μ) and from 0.3321 to 0.3244 for M(E_g), indicating a gradual shift toward slight metallic-like electronic behavior with increasing Nd^{3+} content; however, since it is less than unity, the samples are still non-metallic. This indicates that increasing Nd^{3+} incorporation may promote a greater tendency toward metallic character in the electronic structure of the samples. This trend is consistent with the decrease in optical band gap (E_g) and the simultaneous increase in molar refractivity (R_m) and electronic polarizability (α_m) with increasing Nd^{3+} content, since a narrower band gap and enhanced polarizability both indicate a reduction in the strength of electron localization and a corresponding increase in the mobility of the conduction electrons. Although all the samples remain fundamentally insulating in character (consistent with the general behaviour of spinel ferrites), the systematic decrease in M with Nd^{3+} substitution reflects a progressive narrowing of the effective electronic confinement, correlating with the enhanced dielectric and optical polarizability observed across the series.

3.14. Optical Basicity (Λ_{th})

Optical basicity is an important descriptor of redox behaviour of oxides, as it reflects the electron-donating ability of oxygen ions and the electron-accepting tendency of cations. It is influenced by the nature of metal-oxygen bonding, the distribution of electronic charge, and changes in the local structural environment. This parameter provides insight into the interactions between constituent ions and the electronic properties of oxide systems. The optical basicity of the investigated samples was estimated using Duffy's theoretical approach.[38]

$$\Lambda_{th} = \sum X_i \Lambda_i \tag{25}$$

Here Λ_i denotes the optical basicity of an individual constituent oxide, while Xi represents its molar fraction in the material. The calculation takes into account the Pauling electronegativity of the constituent elements, following the procedure described in the relevant literature. The calculated optical basicity values are listed in Table 4 and exhibit an increasing trend with increasing Nd^{3+} concentration. This behaviour can be interpreted in terms of the Lewis acid-base concept, in which the theoretical optical basicity Λ_{th} of CaO is assigned a reference value of unity for comparison with other oxide materials. In the present case, the pristine sample (x = 0.00) possesses Λ_{th} = 0.780, and this value increases progressively to Λ_{th} = 0.814 for the highest Nd^{3+}-substituted sample (x = 0.25). According to this theory, all the samples in the present series can be regarded as relatively acidic in

character (since $\Lambda_{th} < 1$), with the acidity progressively diminishing (*i.e.*, basicity increasing) as Nd^{3+} content increases. The rise in optical basicity may be attributed to the enhanced charge on oxygen atoms, arising from the substitution of Fe^{3+} by the less electronegative and larger Nd^{3+} ion, which results in greater ionic (less covalent) character of the cation-oxygen bonding. An increase in optical basicity signifies an increased ability of the oxide ions to donate electrons to the surrounding cations, consistent with the progressive modification of the local metal-oxygen environment discussed earlier [39].

3.15. Optical Packing Density (OPD)

The optical packing density varies only slightly from 88.241 to 88.087 across the investigated compositions, as shown in **Table 4**. OPD provides information about the compactness of the optically active constituents within the material and can be used to assess whether substitution produces a major change in the overall structural packing.

$$OPD = n\frac{\rho}{M_w} \times 1000 \tag{26}$$

The near-constant OPD suggests that the fundamental oxygen-based framework of the spinel ferrite remains comparatively stable despite progressive Nd substitution. In other words, the incorporation of the larger Nd^{3+} ion modifies the local cationic environment and optical response without producing a large change in the overall optical packing of the structure. This behavior is significant because the pronounced variations in refractive index, polarizability and dielectric response therefore occur without a corresponding large change in OPD. The optical evolution can consequently be associated more strongly with local electronic and cation-oxygen modifications than with a major collapse or rearrangement of the overall structural framework.

3.16. Overall Physical Correlation of the Optical Parameters

The optical parameters exhibit a mutually consistent evolution with increasing Nd concentration. Nd^{3+} substitution introduces a substantial ionic-radius mismatch relative to Fe^{3+}, producing local structural distortion and modifying the metal-oxygen environment. These structural changes can influence defect-associated and localized electronic states and thereby contribute to the progressive reduction in optical band gap from 2.206 to 2.105 eV. The reduction in E_g is accompanied by an increase in refractive index, molar refractivity, electronic and dielectric polarizability, optical dielectric constant and optical susceptibility. These correlated trends indicate an enhanced electronic response to the optical field. As μ increases, the velocity of light within the material decreases, and the surface reflectivity increases. At the same time, the increase in absorption coefficient contributes to lower optical transmission. Thus, the optical evolution of $ZnNd_xFe_{2-x}O_4$ can be described as a coupled consequence of compositional substitution, local structural perturbation, modified metal-oxygen interactions

and changes in electronic polarizability. The calculated parameters should be regarded as mutually supporting descriptors derived from the measured structural and optical quantities, rather than as independent direct measurements of electronic structure.

4. Conclusion

The current study reveals that substituting Nd^{3+} ions into $ZnFe_2O_4$ ferrite nanoparticles causes systematic, consistent changes in the optical properties of the material. The optical band gap energy decreased gradually from 2.206 to 2.105 eV with increasing Nd^{3+} concentration, which may be associated with the influence of Nd^{3+}-related 4f states below the conduction band and the possible enhancement of charge-transfer processes, leading to a reduction in the effective optical band gap. The latter effect was found to be the driving force for all the following trends, namely, that the refractive index, molar refractivity, electronic polarizability, polarizability of the dielectric, optical dielectric constant, and optical susceptibility consistently increased with the Nd^{3+} content x. At the same time, the velocity of light propagation in the medium and the metallization criterion decreased. Indeed, the gradual rise of the reflection and reflection loss, together with a drop in transmittance, suggested that at higher x, the interaction of the irradiating electromagnetic field with the sample matrix intensified, which in turn corresponded to the enhanced absorption coefficient. The increase in optical basicity with the rise of x testified to the more ionic character of the bonding in the modified zinc ferrite system. On the contrary, the oxygen packing density appeared to be almost constant for all the studied samples. Considering this, it can be concluded that the optical behavior of the $ZnNd_xFe_{2-x}O_4$ ferrite nanoparticles is governed by both optical band gap engineering and the contribution of the individual metal-oxygen bonds, instead of the overall change in the host lattice structure. Therefore, based on the possibility of optical band gap tuning and the enhanced polarizability of the modified system, the application of the obtained ferrite nanoparticles in optical sensors and photovoltaic devices can be proposed; however, it would require experimental verification through the direct assessment of the dielectric properties, particularly the photocatalytic performance, of the composite.

Acknowledgments

The authors thank the Registrar, JNTU Hyderabad; the Chairman, Vice-Chancellor, Malla Reddy University; and the Director, MRCE, Maisammaguda, Dulapally, Hyderabad, for their support.

Author Contributions

Shashi Kumar Jakkaraju: Investigation, Data Curation, Writing—Original Draft.

Katrapally Vijaya Kumar: Conceptualization, Methodology, Critical Revision, Supervision.

Conflicts of Interest

The authors declare no conflicts of interest regarding the publication of this paper.

References

[1] Barde, N.P., Shewale, S.S., Solanki, P.S., Shah, N.A. and Bardapurkar, P.P. (2021) Effect of Silica Matrix on Structural, Optical and Electrical Properties of $Li_{0.5}Fe_{2.5}O_4$ Nanoparticles. *Scripta Materialia*, **194**, Article ID: 113712. https://doi.org/10.1016/j.scriptamat.2020.113712

[2] Pawar, C.S., Gujar, M.P. and Mathe, V.L. (2016) Optical Properties of Spin-Deposited Nanocrystalline Ni-Zn Ferrite Thin Films Processed by Sol-Gel. *Journal of Superconductivity and Novel Magnetism*, **30**, 615-625. https://doi.org/10.1007/s10948-016-3720-y

[3] Dimitrov, V. and Komatsu, T. (2010) An Interpretation of Optical Properties of Oxides and Oxide Glasses in Terms of the Electronic Ion Polarizability and Average Single Bond Strength. *Journal of Chemical Technology and Metallurgy*, **45**, 219-250.

[4] Halimah, M.K., Faznny, M.F., Azlan, M.N. and Sidek, H.A.A. (2017) Optical Basicity and Electronic Polarizability of Zinc Borotellurite Glass Doped La^{3+} Ions. *Results in Physics*, **7**, 581-589. https://doi.org/10.1016/j.rinp.2017.01.014

[5] Mohammadi Badizi, A. and Maleki, H. (2021) One-Step Combustion Synthesis of Sio_2-$CoFe_2O_4$ Nanocomposites and Characterization for Structural, Thermal, Optical and Magnetic Properties. *Materials Science in Semiconductor Processing*, **124**, Article ID: 105594. https://doi.org/10.1016/j.mssp.2020.105594

[6] Wahsh, M.M.S., Othman, A.G.M., Awad, K.R., Girgis, E., Mabrouk, M.R. and Morsy, F.A. (2019) Synthesis and Magneto-Optical Properties of Cobalt Ferrite/Silica Nanoparticles Doped with Cd^{2+} Ions. *Main Group Chemistry*, **18**, 397-410. https://doi.org/10.3233/mgc-180769

[7] Hussain, A., Khalid, M., Chandio, A.D., Yasin, M., Abbas, N., Ashiq, M.G.B., *et al.* (2023) Dielectrically Modified Nd^{3+} Doped (Ni-Mn) Based Spinel Ferrite $Ni_{0.5}Mn_{0.5}Nd_xFe_{2-X}O_4$ Nanoparticles for Energy Storage Applications. *Physica B: Condensed Matter*, **666**, Article ID: 415135. https://doi.org/10.1016/j.physb.2023.415135

[8] Devi, E.C. and Soibam, I. (2017) An Investigation on the Optical Band Gap and Ac Conductivity of Mn-Zn Nanoferrites. *Journal of Superconductivity and Novel Magnetism*, **31**, 1183-1188. https://doi.org/10.1007/s10948-017-4294-z

[9] Chandekar, K.V., Shkir, M. and AlFaify, S. (2020) Tuning the Optical Band Gap and Magnetization of Oleic Acid Coated $CoFe_2O_4$ NPs Synthesized by Facile Hydrothermal Route. *Materials Science and Engineering: B*, **259**, Article ID: 114603. https://doi.org/10.1016/j.mseb.2020.114603

[10] Chandekar, K.V., Shkir, M., Al-Shehri, B.M., AlFaify, S., Halor, R.G., Khan, A., *et al.* (2020) Visible Light Sensitive Cu Doped ZnO: Facile Synthesis, Characterization and High Photocatalytic Response. *Materials Characterization*, **165**, Article ID: 110387. https://doi.org/10.1016/j.matchar.2020.110387

[11] Chandekar, K.V., Alshahrani, T., Ben Gouider Trabelsi, A., Alkallas, F.H., Shkir, M. and AlFaify, S. (2020) Novel Rare Earth Yttrium Doping Effect on Physical Properties of Pbs Nanostructures: Facile Synthesis and Characterization. *Journal of Materials Science*, **56**, 4763-4781. https://doi.org/10.1007/s10853-020-05539-w

[12] Chowdhury, S., Mandal, P. and Ghosh, S. (2019) Structural Properties of Er^{3+} Doped Lead Zinc Phosphate Glasses. *Materials Science and Engineering: B*, **240**, 116-120.

https://doi.org/10.1016/j.mseb.2019.01.014

[13] Widanarto, W., Sahar, M.R., Ghoshal, S.K., Arifin, R., Rohani, M.S., Hamzah, K., *et al.* (2013) Natural Fe_3O_4 Nanoparticles Embedded Zinc-Tellurite Glasses: Polarizability and Optical Properties. *Materials Chemistry and Physics*, **138**, 174-178. https://doi.org/10.1016/j.matchemphys.2012.11.040

[14] Barde, N.P., Solanki, P.S., Shah, N.A. and Bardapurkar, P.P. (2022) Investigations on Structural, Magnetic, Elastic and Thermodynamic Properties of Lithium Ferrite-Silica Nanocomposites. *Journal of Molecular Structure*, **1260**, Article ID: 132771. https://doi.org/10.1016/j.molstruc.2022.132771

[15] Bhatia, B., Meena, S.L., Parihar, V. and Poonia, M. (2015) Optical Basicity and Polarizability of Nd^{3+}-Doped Bismuth Borate Glasses. *New Journal of Glass and Ceramics*, **5**, 44-52. https://doi.org/10.4236/njgc.2015.53006

[16] Jakkaraju, S.K. and Kumar, K.V. (2026) Role of Nd^{3+} Ions in Modulating Structural, Thermal, Magnetic and Antibacterial Properties of $ZnFe_2O_4$ Nanoferrite. *Inorganic Chemistry Communications*, **194**, Article ID: 117495. https://doi.org/10.1016/j.inoche.2026.117495

[17] Vinod, G., Rajashekhar, K. and Naik, J.L. (2023) Dysprosium Doped $Cu_{0.8}Cd_{0.2}Dy_xFe_{2-x}O_4$ Nano Ferrites: A Combined Impact of Dy^{3+} on Enhanced Physical, Optical, Magnetic, and DC-Electrical Properties. *Ceramics International*, **49**, 2829-2851. https://doi.org/10.1016/j.ceramint.2022.09.265

[18] Nguyen, L.T.T., Nguyen, H.T.T., Le, T.H., Nguyen, L.T.H., Nguyen, H.Q., Pham, T.T.H., *et al.* (2021) Enhanced Photocatalytic Activity of Spherical Nd^{3+} Substituted $ZnFe_2O_4$ Nanoparticles. *Materials*, **14**, Article 2054. https://doi.org/10.3390/ma14082054

[19] Patil, S.B., Bhojya Naik, H.S., Nagaraju, G., Viswanath, R. and Rashmi, S.K. (2017) Synthesis of Visible Light Active Gd^{3+}-Substituted $ZnFe_2O_4$ Nanoparticles for Photocatalytic and Antibacterial Activities. *The European Physical Journal Plus*, **132**, Article No. 328. https://doi.org/10.1140/epjp/i2017-11602-x

[20] Jakkaraju, S.K. and Kumar, K.V. (2026) Gd^{3+}-Substituted $ZnFe_2O_4$ Spinel Nanoferrites: Structural, Optical, Magnetic and Antibacterial Characteristics. *Phase Transitions*. https://doi.org/10.1080/01411594.2026.2730635

[21] Jdey, W., Hamdaoui, N., Hcini, S., Mansouri, S. and El Mir, L. (2024) Enhancement of the Optical Properties of $Mg_{0.6}Cu_{0.4}FeCrO_4$ Spinel Ferrite via Heat Treatment. *Optical Materials*, **147**, Article ID: 114666. https://doi.org/10.1016/j.optmat.2023.114666

[22] Chebbi, M., Mansouri, S., Hcini, S., Ghiloufi, I., Mimouni, A. and Mir, L.E. (2024) Investigating the Impact of Calcination Temperature on the Structural and Optical Properties of Chromium-Substituted Mg-Co Ferrite Nanoparticles. *Journal of Molecular Structure*, **1295**, Article ID: 136740. https://doi.org/10.1016/j.molstruc.2023.136740

[23] Ayman, I., Aadil, M., Shahid, M., Khalid, A., Samama, H., Somaily, H.H., *et al.* (2024) Wet Synthesis of Magnetically Retrievable Mn/Nd Co-Doped Cobalt Ferrites for Visible Light-Driven Photocatalytic Annihilation of Azo Dye. *Materials Science in Semiconductor Processing*, **178**, Article ID: 108462. https://doi.org/10.1016/j.mssp.2024.108462

[24] Qaid, S.M.H., Al-Asbahi, B.A., Ghaithan, H.M., AlSalhi, M.S. and Al Dwayyan, A.S. (2020) Optical and Structural Properties of $CsPbBr_3$ Perovskite Quantum Dots/PFO Polymer Composite Thin Films. *Journal of Colloid and Interface Science*, **563**, 426-434. https://doi.org/10.1016/j.jcis.2019.12.094

[25] Rekaby, M., Ahmed, M., Awad, R., El Sayed, M.Y., Abu-Saied, M.A. and Abou-Aly, A.I. (2026) Tailoring the Microstructure, Optical, and Magnetic Characteristics of $Co_{0.6}Zn_{0.4}Fe_2O_4$ Nanoferrites through Ni^{2+}-Al^{3+} Co-Doping. *Scientific Reports*, **16**, Article No. 14046. https://doi.org/10.1038/s41598-026-46866-3

[26] Fadhalaoui, A., Kouass, S. and Dhaouadi, H. (2017) $Bi_xCe_{1-x}PO_4$ (x = 0.00, 0.02, and 0.08) Nanorods: Structural, Electrical, Optical, and Electrochemical Properties. *Ionics*, **24**, 429-450. https://doi.org/10.1007/s11581-017-2222-7

[27] Korsakov, A., Salimgareev, D., Lvov, A. and Zhukova, L. (2017) IR Spectroscopic Determination of the Refractive Index of $Ag_{1-x}Tl_xBr_{1-0.54x}I_{0.54x}$ ($0 \leqslant X \leqslant 0.05$) Crystals. *Optics & Laser Technology*, **93**, 18-23. https://doi.org/10.1016/j.optlastec.2017.01.030

[28] Anani, M., Mathieu, C., Lebid, S., Amar, Y., Chama, Z. and Abid, H. (2008) Model for Calculating the Refractive Index of a III-V Semiconductor. *Computational Materials Science*, **41**, 570-575. https://doi.org/10.1016/j.commatsci.2007.05.023

[29] Tripathy, S.K. (2015) Refractive Indices of Semiconductors from Energy Gaps. *Optical Materials*, **46**, 240-246. https://doi.org/10.1016/j.optmat.2015.04.026

[30] Soharab, M., Bhaumik, I., Bhatt, R., Saxena, A. and Karnal, A.K. (2019) Effect of Nd Doping on the Refractive Index and Thermo-Optic Coefficient of $GdVO_4$ Single Crystals. *Applied Physics B*, **125**, Article 84. https://doi.org/10.1007/s00340-019-7194-z

[31] Jakkaraju, S.K., Kumar, K.V. and Kumar, N.H. (2025) Influence of Calcination Temperature on Gadolinium Doped Magnesium-Zinc Ferrite Nanoparticles: Structural, Optical, and Photocatalytic Properties for Water Splitting Applications. *Next Materials*, **8**, Article ID: 100705. https://doi.org/10.1016/j.nxmate.2025.100705

[32] Hisatomi, T., Wang, Q., Zhang, F., Ardo, S., Reisner, E. and Nishiyama, H., *et al.* (2024) Photocatalytic Water Splitting for Large-Scale Solar-to-Chemical Energy Conversion and Storage. *Frontiers in Science*, **2**, Article ID: 1411644. https://doi.org/10.3389/fsci.2024.1411644

[33] Modi, K.B., Shah, S.J., Pujara, N.B., Pathak, T.K., Vasoya, N.H. and Jhala, I.G. (2013) Infrared Spectral Evolution, Elastic, Optical and Thermodynamic Properties Study on Mechanically Milled $Ni_{0.5}Zn_{0.5}Fe_2O_4$ Spinel Ferrite. *Journal of Molecular Structure*, **1049**, 250-262. https://doi.org/10.1016/j.molstruc.2013.06.051

[34] Modi, K.B., Raval, P.Y., Pansara, P.R., Badi, I.R., Devmurari, D.R., Munshi, S.S., *et al.* (2016) On the Relationship between Structural-Optical Parameters of $Y_{3-x}Fe_{5+x}O_{12}$ Garnet Ferrites and the Oxide Additivity Rule. *Journal of Superconductivity and Novel Magnetism*, **29**, 1931-1936. https://doi.org/10.1007/s10948-016-3488-0

[35] Barde, N.P., Rathod, V.R., Solanki, P.S., Shah, N.A. and Bardapurkar, P.P. (2022) On the Structural, Refractive Index and Energy Bandgap Based Optical Properties of Lithium Ferrite Nanoparticles Dispersed in Silica Matrix. *Applied Surface Science Advances*, **11**, Article ID: 100302. https://doi.org/10.1016/j.apsadv.2022.100302

[36] Shannon, R.D. and Fischer, R.X. (2006) Empirical Electronic Polarizabilities in Oxides, Hydroxides, Oxyfluorides, and Oxychlorides. *Physical Review B*, **73**, Article ID: 235111. https://doi.org/10.1103/physrevb.73.235111

[37] Umar, S.A., Halimah, M.K., Chan, K.T. and Latif, A.A. (2017) Polarizability, Optical Basicity and Electric Susceptibility of Er^{3+} Doped Silicate Borotellurite Glasses. *Journal of Non-Crystalline Solids*, **471**, 101-109. https://doi.org/10.1016/j.jnoncrysol.2017.05.018

[38] Duffy, J.A. (1996) Optical Basicity: A Practical Acid-Base Theory for Oxides and Oxyanions. *Journal of Chemical Education*, **73**, 1138. https://doi.org/10.1021/ed073p1138

[39] Azis, M.N.A., Kamari, H.M., Zulkefly, S.S. and Yusoff, W.D.W. (2014) Polarizability and Optical Basicity of Er^{3+} Ions Doped Tellurite Based Glasses. *Chalcogenide Letters*, **11**, 319-335. https://api.semanticscholar.org/CorpusID:97542740